
Audio-to-Image Cross-Modal Generation

Maciej Żelaszczyk¹ Jacek Mańdziuk¹

Abstract

Cross-modal representation learning allows to integrate information from different modalities into one representation. At the same time, research on generative models tends to focus on the visual domain with less emphasis on other domains, such as audio or text, potentially missing the benefits of shared representations. Studies successfully linking more than one modality in the generative setting are rare. In this context, we verify the possibility to train variational autoencoders (VAEs) to reconstruct image archetypes from audio data. Specifically, we consider VAEs in an adversarial training framework in order to ensure more variability in the generated data and find that there is a trade-off between the consistency and diversity of the generated images - this trade-off can be governed by scaling the reconstruction loss up or down, respectively. Our results further suggest that even in the case when the generated images are relatively inconsistent (diverse), features that are critical for proper image classification are preserved.

1. Introduction

In representation learning, a frequent goal is to find a mapping from the data space (e.g. a space of images) to a more compact latent space, which is not directly observable (an embedding space / feature space). One of the main assumptions underlying such a process is that real data can be reliably summarized by a relatively limited set of factors. These factors correspond to elements of the latent / embedding / feature vectors. The resulting reduction of dimensionality facilitates the use of latent vectors for a range of tasks, such as classification or compression. Latent vectors are also frequently used in generative models, which often utilize random latent vectors in the process of data generation.

¹Faculty of Mathematics and Information Science, Warsaw University of Technology, Warsaw, Poland. Correspondence to: Maciej Żelaszczyk <m.zelaszczyk@mini.pw.edu.pl>, Jacek Mańdziuk <mandziuk@mini.pw.edu.pl>.

Regardless of the actual application, most of representation learning research is focused on data from one modality (e.g. image, text, audio, etc.). For instance, image classification or generation tasks usually use data solely from the image modality. Despite the success of such applications, it seems that limiting oneself to data from one modality is not a realistic model for deep learning. Real-world objects usually generate data from more than one modality and humans perceive the world around them through more than just one sense. A significant portion of the objects we interact with can be identified based on data from multiple senses. In particular, it is usually possible to imagine an object based on only one source of sensory information (e.g. imagining a car based on the sound of its engine), which suggests the possibility of learning a common representation of an object integrating information from multiple modalities. Such a representation could then plausibly be matched to data from just one modality and the missing modalities could be inferred.

The process of learning such common representations would be facilitated by the temporal alignment of data from multiple modalities. In such a setting, sensory information from different modalities appears together and this link between multiple modalities enables learning without additional supervision. In this work, we aim to highlight the possibility of learning shared representations from cross-modal (multi-modal) data due to the temporal alignment of datasets.

Our contributions:

- We construct audio-image datasets and show that it is possible to generate images based on audio data, as audio features overlap with visual features to an extent that makes image generation possible.
- We discuss how the data alignment process influences the generation process. Many-to-one mappings result in data *archetypes*, while one-to-one mappings ensure more variability in the data.
- We analyze how scaling the reconstruction loss up or down influences the properties of the generated data.
- We quantitatively assess the degree to which transition between audio and image data preserves relevant visual features.

2. Related work

This work is related to several strands of research, which include representation learning, joint latent space learning, input reconstruction and cross-modal learning.

Representation learning is addressed by [Hinton et al. \(1986\)](#) who discuss the possibility of representing a concept as an activity pattern in more than one computing element within a network of such elements - a *distributed representation*. They argue that such representations could potentially achieve content-addressable memory and generalization capabilities. [Schmidhuber \(1992\)](#) proposes that statistical independence of parts of the representation should be a goal of unsupervised learning. [Bengio et al. \(2013\)](#) restate this in the form of *disentangled* factors of variation, motivate the importance of representation learning, and provide a review of success stories involving representation learning. They explicitly hypothesize that representations might be partially shared for different tasks or domains and that this might be beneficial in *transfer learning*, *domain adaptation* or *multi-task learning*.

In reference to cross-modal learning and joint latent space learning, [Weston et al. \(2010\)](#) train a method to learn a joint embedding space for both images and their annotations. [Arandjelovic & Zisserman \(2017\)](#) and [\(2018\)](#) show that it is possible to jointly learn audio and visual representations from an aligned audio-visual dataset with no additional supervision. The representations from the audio and visual modalities can then be compared to localize objects potentially linked to the sound and vice versa. [Xing et al. \(2019\)](#) combine information from visual and semantic feature spaces to improve model performance in a few-shot learning setting. [Li et al. \(2019\)](#) present the existence of adversarial examples for cross-modal text/image data and show that adversarial training can improve the robustness of a cross-modal hashing network. [Wen et al. \(2019\)](#) present an architecture capable of learning a shared representation for voices and faces by mapping them to their common covariates. [Lu et al. \(2019\)](#) learn task-agnostic joint representations of images and natural language. In a video setting, [Sun et al. \(2019\)](#) combine video data and text produced by speech-recognition methods to learned high-level *linguistic features*.

In the context of input reconstruction, [Ackley et al. \(1985\)](#) pose an encoder problem where input should be reconstructed in spite of a sparse representation, while [Rumelhart et al. \(1986\)](#) show that it is possible to train a neural network with an intermediate bottleneck layer in an unsupervised manner to reconstruct input, an idea further developed in [\(Bourlard & Kamp, 1988\)](#), [\(Kramer, 1991\)](#), [\(Hinton & Zemel, 1993\)](#) and [\(Vincent et al., 2008\)](#). [Kingma & Welling \(2014\)](#) use a mapping from the input to the parameters of a multidimensional normal distribution in a variational au-

toencoder (VAE) architecture. This facilitates the process of generating new data from latent space representations without the corresponding input data. Extensions incorporating discrete latent codes ([van den Oord et al., 2017](#)) have also been proposed, resulting in images of increasing size ([Razavi et al., 2019](#)).

A different line of generative models has been triggered by [Goodfellow et al. \(2014\)](#), who proposed a generative adversarial network (GAN) framework. This framework relies on game-theoretic ideas and jointly trains two neural networks with opposing objectives in order for one of the networks to learn to generate data similar but not identical to examples from the train dataset. The GAN architecture has been extended, for instance to learn a mapping from data space to the latent space ([Donahue et al., 2017](#)) or handle images of higher resolution ([Brock et al., 2019](#)). While GANs tend to produce sharper images than VAEs, significant instabilities in adversarial training have been identified and various approaches to stabilize training have been proposed ([Radford et al., 2016](#)), ([Arjovsky et al., 2017](#)), ([Miyato et al., 2018](#)), with no approach conclusively resolving the issue so far.

There is also a growing body of research on cross-modal generative models. [Oord et al. \(2016\)](#) train a generative model conditioned on *linguistic features* extracted from text input for the text-to-speech task. Conditional GANs are used to generate images from text in ([Reed et al., 2016](#)). The tasks of generating images from audio and generating audio from images are tackled in an adversarial setting in ([Chen et al., 2017](#)). [Hao et al. \(2018\)](#) extend the adversarial framework to generate audio and visual data mutually. [Hsu & Glass \(2018\)](#) train a modified VAE to incorporate not only shared factors but also modality-dependent ones for audio/image datasets. [Shi et al. \(2019\)](#) employ a cross-modal VAE to generate images from text and text from images. [Müller-Eberstein & van Noord \(2019\)](#) show that, with pre-training, VAEs can be recombined to generate audio from images and that the produced audio is at least somewhat consistent with human notions of similarity between the audio and images, even in the absence of aligned datasets.

While research on cross-modal generative models has advanced significantly, it is still very much underdeveloped. Most of this area focuses on linking the linguistic domain with the audio domain (e.g. text to speech) or providing a bridge between the linguistic and the visual domains (e.g. image captions, text-to-image generation). At present, the audio-visual branch is underrepresented within the broader cross-modal generative current. In spite of the development of cross-modal methods, relatively little research on audio-visual architectures has been published. Even less research has been conducted directly on audio-to-image generation. Relative to image datasets, audio-visual datasets are few and far between.

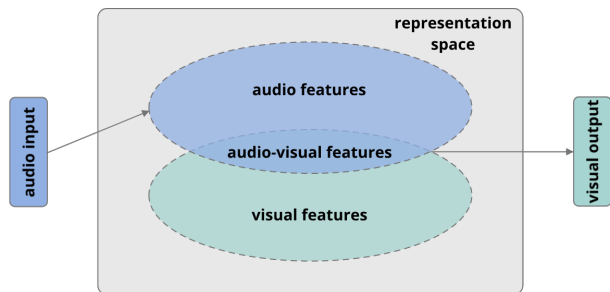


Figure 1. Relationship between audio and visual features.

In this context we strive to align audio and image datasets in order to facilitate the process of audio-to-image generation. We also propose methods to extract audio features and utilize their subset, the *audio-visual features*, to produce images consistent with the ones observed in the data space. These methods differ from the standard supervised conditional variational autoencoder or conditional generative adversarial network setups (Goodfellow et al., 2014). Our work is a potential starting point for research on the possibility of utilizing variational autoencoders in an adversarial setting for audio-visual generation. It is also the first study we are aware of concerned with many-to-one vs. one-to-one mappings for cross-modal dataset alignment and the effects of these mappings on the generated data. Our work points to a new potential area of research related to precise methods of set alignment and how they can impact the data generation process. In particular, many-to-one mappings may be preferable for some tasks, and vice versa.

3. Generative models

For two variables \mathbf{x} , \mathbf{y} , a *generative model* is one which describes the joint probability distribution $p(\mathbf{x}, \mathbf{y})$. In machine learning applications, the model can be written as $p(\mathbf{x}, \mathbf{z})$, where \mathbf{x} comes from the *data space*, e.g. the space where we can observe the data, and \mathbf{z} comes from the *latent space*, a directly unobservable space of features.

3.1. Variational autoencoders (VAEs)

VAEs (Kingma & Welling, 2014) extend the autonecoder architecture. Let us consider the generative model $p_\theta(\mathbf{z})p_\theta(\mathbf{x}|\mathbf{z})$, and $q_\phi(\mathbf{z}|\mathbf{x})$ be the approximation of the true intractable posterior $p_\theta(\mathbf{z}|\mathbf{x})$. We may refer to $q_\phi(\mathbf{z}|\mathbf{x})$ as a probabilistic *encoder* and to $p_\theta(\mathbf{x}|\mathbf{z})$ as a probabilistic *decoder*. Let $p_\theta(\mathbf{x}|\mathbf{z})$ and $q_\phi(\mathbf{z}|\mathbf{x})$ be neural networks parametrized by θ and ϕ , respectively. Let \mathbf{z} be a random variable and $\mathbf{z} = g_\theta(\mathbf{x}, \epsilon)$, where ϵ is an auxiliary variable with an independent marginal and g_θ is a function parametrized by θ . We can sample from the posterior $\mathbf{z}^{(i)} \sim q_\phi(\mathbf{z}|\mathbf{x}^{(i)})$, calculating $\mathbf{z}^{(i)} = g_\theta(\mathbf{x}^{(i)}, \epsilon) = \mu^{(i)} + \sigma^{(i)} \odot \epsilon$,

where $\epsilon \sim \mathcal{N}(\mathbf{0}, \mathbf{I})$. The loss function for a given data example can be expressed as:

$$\mathcal{L}(\mathbf{x}^{(i)}, \theta, \phi) = -\mathbb{E}_{\mathbf{z} \sim q_\phi(\mathbf{z}|\mathbf{x}^{(i)})} \left[\log p_\theta(\mathbf{x}^{(i)}|\mathbf{z}) \right] + \mathbb{KL}(q_\phi(\mathbf{z}|\mathbf{x}^{(i)})||p(\mathbf{z})) \quad (1)$$

where \mathbb{KL} is the Kullback–Leibler divergence.

In practice, the process of training a VAE consists of passing data through the encoder, which maps to parameter vectors μ and σ . These vectors are then combined with a random ϵ vector sampled from the standard normal distribution via the equation $\mathbf{z}^{(i)} = \mu^{(i)} + \sigma^{(i)} \odot \epsilon$. Thanks to the reparametrization trick, the model is differentiable and can be trained with backpropagation. It is worth noting that the loss formulation consists of two terms: the *reconstruction error* and the KL divergence. While the reconstruction loss encourages adhering to examples seen in the dataset, the KL divergence ensures that the encoder remains consistent with the standard normal distribution assumed for $p(\mathbf{z})$. Such an assumption simplifies sampling from a trained model.

3.2. Generative adversarial networks (GANs)

GANs, first introduced in (Goodfellow et al., 2014), apply the concept of a minimax game to generative models. In this setting, we consider two neural networks, the *generator* $G(\mathbf{z})$ and the *discriminator* $D(\mathbf{x})$. We define a latent space prior $p_z(\mathbf{z})$. G maps from the latent space to the data space, while D maps from the data space to a scalar output, which represents the probability that a sample comes from the data space rather than that it has been produced by G . G and D are trained in turns, essentially playing a two-player minimax game:

$$\min_G \max_D V(D, G) = \mathbb{E}_{\mathbf{x} \sim p_{data}(\mathbf{x})} [\log(D(\mathbf{x}))] + \mathbb{E}_{\mathbf{z} \sim p_z(\mathbf{z})} [\log(1 - D(G(\mathbf{z})))] \quad (2)$$

This minimax game has a global optimum for $p_g = p_{data}$, i.e. for G generating images indistinguishable from the ones in the data space and D continually producing $\frac{1}{2}$ as its assessment of the probability that the samples come from the data distribution. This global optimum can theoretically be achieved via backpropagation in sequential weight updates for both networks. In reality, the training process for GANs is frequently unstable and convergence is by no means automatic.

4. Audio-to-Image Architectures

We consider two generative setups geared towards extracting audio representations from sound and using a subset of these features relevant for the visual domain, the *audio-visual*

features, for image generation (Figure 1). Our first model is a modification of the classic VAE architecture. Our second architecture is a combination of a VAE and a GAN network. We use VAE as the GAN generator and train the whole system adversarially. Both architectures are presented in Figure 2.

4.1. Audio-to-Image VAE

We modify the VAE encoder to process audio data and map it to the parameters of the latent space. It now describes a distribution $q_\phi(\mathbf{f}|\mathbf{a})$, where \mathbf{a} represents the audio input and \mathbf{f} denotes the *audio-visual features* - features from the audio space, which would be relevant for image generation. These features are used as parameters μ and σ in the process of generating random vectors $\mathbf{f}^{(i)} = \mu^{(i)} + \sigma^{(i)} \odot \epsilon$, in line with the classic VAE architecture. The random vectors are then passed through the decoder $p_\theta(\mathbf{i}|\mathbf{f})$, which maps to the image space. The loss minimized in training is:

$$\mathcal{L}(\mathbf{a}^{(i)}, \mathbf{i}^{(i)}, \theta, \phi) = -\mathbb{E}_{\mathbf{f} \sim q_\phi(\mathbf{f}|\mathbf{a}^{(i)})} [\log p_\theta(\mathbf{i}^{(i)}|\mathbf{f})] + \mathbb{KL}(q_\phi(\mathbf{f}|\mathbf{a}^{(i)})||p(\mathbf{f})) \quad (3)$$

The whole architecture is trained with backpropagation just like a vanilla VAE. However, the Audio-to-Image VAE (AIVAE) requires two aligned data sources, as each training example is a tuple $(\mathbf{a}^{(i)}, \mathbf{i}^{(i)})$.

4.2. Audio-to-Image VAE-GAN

AIVAE can be further extended in a setting where it is treated as the generator in an adversarial framework, $G(\mathbf{a}) = \text{AIVAE}(\mathbf{a})$. Now, $G : \mathbf{a} \rightarrow \mathbf{i}$, where \mathbf{a} and \mathbf{i} are the audio and image spaces, respectively. The discriminator $D(\mathbf{i})$ tries to discern between real images and the ones manufactured by G . It is worth noting that D does not have explicit access to the pairing between the image and audio and so is not likely to enforce correct classes from G . The information about the pairing $(\mathbf{a}^{(i)}, \mathbf{i}^{(i)})$ is incorporated via a reconstruction loss term in the objective function:

$$\min_G \max_D V(D, G) = \mathbb{E}_{\mathbf{i} \sim p_{data}(\mathbf{i})} \{\log(D(\mathbf{i}))\} + \mathbb{E}_{\mathbf{a} \sim p_{data}(\mathbf{a})} \mathbb{E}_{\mathbf{f} \sim q_\phi(\mathbf{f}|\mathbf{a})} \{\log(1 - D(G(\mathbf{f}))) - \alpha \log p_\theta(\mathbf{i}|\mathbf{f}) + \mathbb{KL}(q_\phi(\mathbf{f}|\mathbf{a})||p(\mathbf{f}))\} \quad (4)$$

This objective function incorporates the opposing goals of G and D , while taking into account the information about the expected reconstruction and desired latent (feature) distribution. The hyperparameter α is designed to regulate the importance of reconstruction vs. adversarial goals. Similarly to the AIVAE setup, the Audio-to-Image VAE-GAN

(AIVAEGAN) loss relies on aligned data without explicit supervision.

5. Experiments

We test AIVAE and AIVAEGAN on two synthetic datasets in order to assess their capability to generate images from audio data.

5.1. Datasets

We construct two synthetic datasets for our experiments. Both of them rely on the MNIST dataset as a source of digit images to be paired with audio data.

5.1.1. MNIST-FSDD

The first dataset combines 28×28 -pixel MNIST digits with audio data from the Free Spoken Digit Dataset (FSDD)¹. FSDD consists of 2 000 WAV files, which are the recorded pronunciations of digits by 4 speakers, which amounts to 50 pronunciations per digit per speaker. We represent the recordings as MEL-scaled spectrograms resized to 48×48 pixels. We then perform a random train/test split, where 90% of the data is assigned to the train set and the remaining 10% of the data is in the test set.

After initial preprocessing, the FSDD data is paired with the MNIST digits in the following procedure. We sample digits from MNIST without replacement and for each of them, we sample with replacement from FSDD spectrograms with matching labels. Each MNIST digit is used once, but each FSDD spectrogram is paired multiple times with various MNIST digits from the corresponding class. This many-to-one MNIST \rightarrow FSDD mapping enforces the alignment of datasets along labels. This is the only time the label information is used prior to evaluation. The outlined steps are repeated separately for the train and test sets. The synthesized dataset consists of 60 000 audio-image pairs for the train set and 10 000 pairs for the test set.

5.1.2. MNIST-SCD

Our second dataset is based on MNIST for image data and on the Speech Commands Dataset (SCD) for audio data². SCD has 65 000 one-second long recordings of 30 words. We limit our analysis to the words representing digits. This leaves us with 23 666 utterances distributed among 10 classes. For simplicity, we will henceforth refer to this subset as *SCD*, having in mind that we consider

¹The FSDD dataset is available at <https://github.com/Jakobovski/free-spoken-digit-dataset>.

²The SCD dataset can be downloaded from <https://ai.googleblog.com/2017/08/launching-speech-commands-dataset.html>.

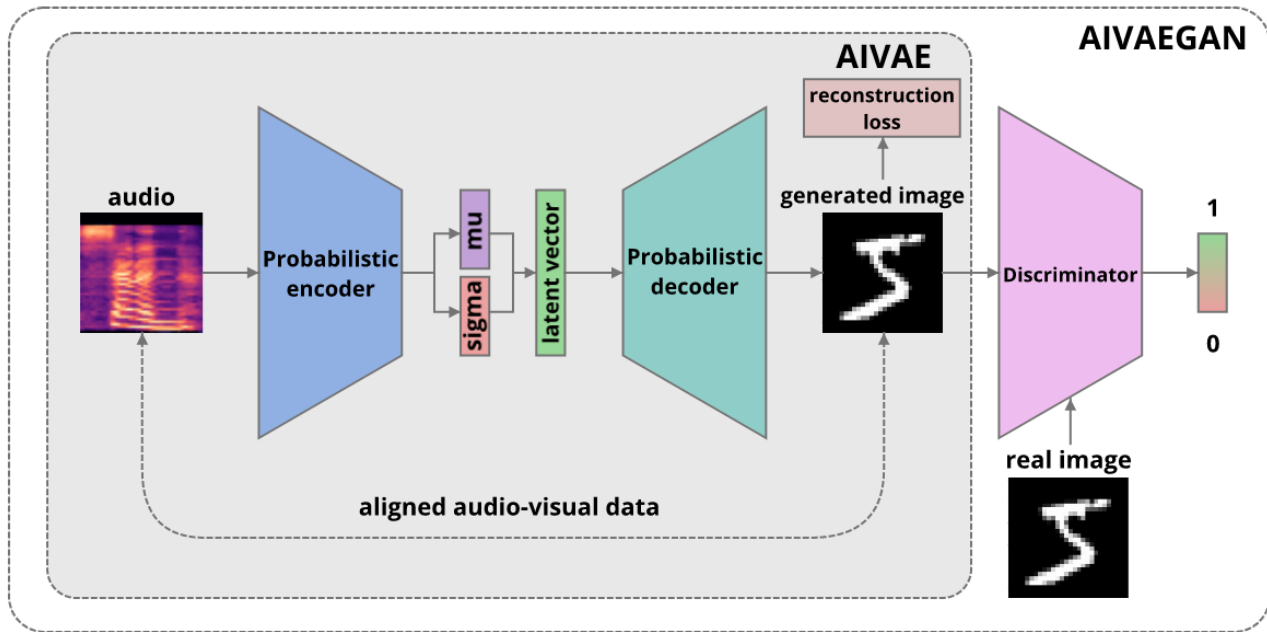


Figure 2. AIVAE and AIVAEGAN architectures.

the digit-related subset of the original dataset. Similarly to the previous case, we convert the WAV files to MEL-scaled spectrograms, resize them to 48×48 pixels and randomly split the dataset so that 90% of the data is used as a train set and 10% is held out for evaluation. We align MNIST and the truncated SCD in a sequential approach. For each class label we randomly sample a spectrogram without replacement and match it to a MNIST image with the same class via random sampling without replacement. This results in a one-to-one MNIST \rightarrow SCD mapping. Again, these steps are performed separately for the train and test sets. The resulting train set is comprised of 21 160 audio-image pairs, while the produced test set consists of 2 360 audio-image pairs.

5.2. Results

We test the AIVAE (Table 1) and AIVAEGAN (Table 2) architectures on the MNIST-FSDD and MNIST-SCD datasets with the latent space dimension set to 64 in each experiment. All models are trained for 100 epochs with batches of 128 examples and are optimized with Adam (Kingma & Ba, 2015). The initial learning rate is set to 10^{-3} for AIVAE and to 2×10^{-4} for both the generator and the discriminator of AIVAEGAN.

5.2.1. QUALITATIVE EVALUATION

We first investigate the reconstruction capabilities of AIVAE for MNIST-FSDD and MNIST-SCD. Figure 3 presents real images from the last epoch of training together with their

Table 1. Audio-to-image variational autoencoder architecture (AIVAE).

AUDIO ENCODER	IMAGE DECODER
INPUT 48X48	INPUT 64
CONV 4X4, 64, STR=2	FC 512
RELU	RELU
CONV 4X4, 128, STR=2	FC 1024
RELU	RELU
FC 1024	FC 7X7X128
RELU	RELU
FC 512	UPCONV 4X4, 64, STR=2
RELU	RELU
μ, σ : FC 64	UPCONV 4X4, 1, STR=2
RELU	SIGMOID
OUTPUT 2X64	OUTPUT 28X28

reconstructions. The classes of the generated images are consistent with their real counterparts for both datasets. The images generated for MNIST-SCD display more variability and less blur, while the ones generated for MNIST-FSDD display a pattern in which each class is represented by visually indistinguishable images - the *archetypes* for each class. The archetypal nature of these images stems from the fact that the MNIST-FSDD dataset was constructed via a many-to-one mapping and each audio data point was associated with multiple digits from the MNIST database. Consequently, for each digit the model has learned its *average* reconstruction.

The reconstructions are further evaluated on the test set

Table 2. Audio-to-image variational autoencoder - generative adversarial network architecture (AIVAEGAN).

AUDIO ENCODER	IMAGE DECODER	DISCRIMINATOR
INPUT 48x48	INPUT 64	INPUT 28x28
CONV 4, 128, 2	UPCONV 3, 512, 2	CONV 4, 128, 2
CONV 4, 256, 2	UPCONV 3, 256, 2	CONV 4, 256, 2
CONV 4, 512, 2	UPCONV 2, 128, 2	CONV 4, 512, 2
μ, σ : CONV 4, 64, 2	UPCONV 2, 1, 2	CONV 1, 1, 1, SIGM
OUTPUT 2x64	OUTPUT 28x28	OUTPUT 1
LEAKYRELU(0.2)	RELU	LEAKYRELU(0.2)
BATCHNORM	BATCHNORM	BATCHNORM

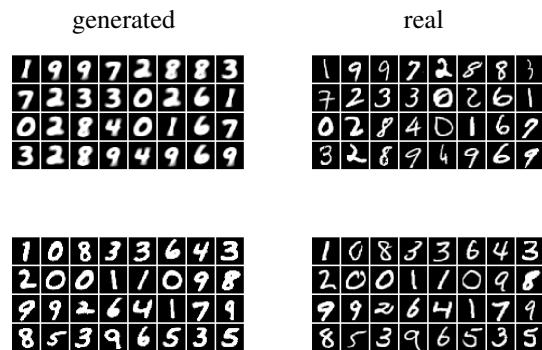
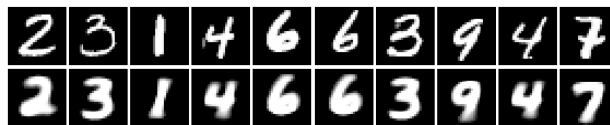


Figure 3. Generated vs. real images at the end of training (AIVAE). Top row: MNIST-FSDD. Bottom row: MNIST-SCD.

with the results presented in Figure 4. These outcomes support the initial idea that the model trained on the many-to-one dataset recovers digit archetypes. The model trained on the one-to-one dataset is less consistent, as evidenced by partially unintelligible reconstructions, however, it does retain reconstruction capabilities and shows more variability in the generated data.

For the AIVAEGAN model, the train-set reconstructions on MNIST-FSDD and MNIST-SCD are presented in Figures 5 and 6, respectively. For MNIST-FSDD, the quality of reconstructions at the end of training is relatively high, with lower levels of α promoting more variation in the generated images. Conversely, for $\alpha = 1$ and $\alpha = 2$, stricter adherence to train data is observed. The results for MNIST-SCD follow the same pattern, however, the one-to-one mapping in this dataset ensures more variability is preserved without necessarily sacrificing the correct labels.

These outcomes are verified on the test sets (Figure 7) and are consistent with our earlier remarks. Lower α levels result in more variation and less adherence to proper classes. Higher values of α result in more archetypical data, however, even for larger α values a one-to-one training set mapping preserves diversity in the generated data.



(a) MNIST-FSDD



(b) MNIST-SCD

Figure 4. Test-set reconstructions for AIVAE. Random, not cherry-picked.

5.2.2. QUANTITATIVE EVALUATION

While eyeball tests confirm the possibility of image generation from audio features for aligned datasets, such a form of inspection is inherently subjective. A quantitative evaluation of the ability of AIVAE and AIVAEGAN to preserve audio features important for image generation would be a more objective measure. To this end, the following procedure is proposed. First, we generate images from audio for the test sets of both MNIST-FSDD and MNIST-SCD. Then, these images are fed to a pretrained MNIST classifier and the accuracy of prediction is recorded. Such a process would allow to assess the extent to which the images generated by our models retain information necessary for image classification.

We choose a LeNet5 classifier (Lecun et al., 1998) - a classic CNN with convolutional/pooling blocks followed by fully-connected layers. The details of the architecture are presented in Table 3. We train it on the MNIST train set for 100 epochs with Adam, with an initial learning rate of 10^{-3} . The network achieves a 98.7% accuracy on the MNIST test set. This is the benchmark we would compare our models against. Intuitively, the accuracy of the pretrained classifier on the data generated by our models should be lower as the audio features used in the data generation process potentially encompass only a subset of the relevant visual features (the *audio-visual features*).

It turns out that for AIVAE the accuracy remains close to 95% for the many-to-one data setting. The one-to-one data alignment results in lower accuracy, albeit still above 85% (see Table 4). AIVAEGAN results display a pattern where for many-to-one data the accuracy of the LeNet5 classifier remains considerably higher than for the one-to-one dataset. At the same time, a higher weight associated with the reconstruction loss improves visual feature retention.

A comparison of AIVAE and AIVAEGAN reveals that the gap in performance between the two models is influenced

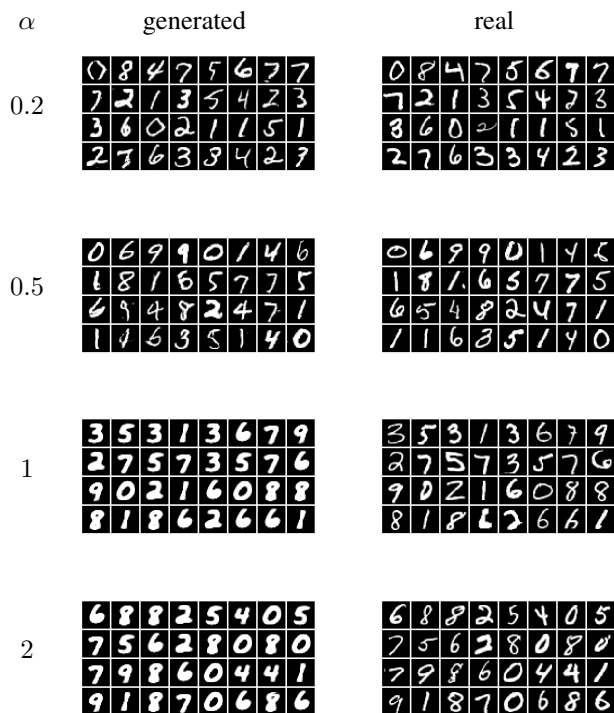


Figure 5. Generated vs. real images at the end of training for different levels of reconstruction loss importance (AIVAEGAN, MNIST-FSDD).

by the level of α set for AIVAEGAN. Higher levels of α result in a smaller difference in performance between the two models, particularly for $\alpha = 2$ and the MNIST-FSDD dataset. This is perhaps not surprising, as the reconstruction loss explicitly enforces stronger adherence to images from the data space. A lower α promotes more diversity in the generated digits, but this comes at a cost of losing visual features distinguishable for a pretrained classifier. It does seem that the effect of the reconstruction loss on the error rate is more pronounced for the many-to-one mapping. Going from $\alpha = 0.2$ to $\alpha = 2$, the error rate drops 44% in the one-to-one setting, while the corresponding drop for the many-to-one setting is 70%. The lower sensitivity of the error rate to changes in α for the one-to-one setting, combined with the less stable adversarial learning process, may also account for a lower top accuracy on MNIST-SCD when comparing AIVAEGAN against AIVAE.

We conduct an additional evaluation of the quality of features of AIVAE trained on MNIST-FSDD and MNIST-SCD. Namely, we randomly set k elements of the latent vector to 0 and record the classification accuracy of the LeNet5 classifier on both test sets. We repeat this for $k \in \{0, 1, \dots, 64\}$. The results are presented in Figure 8. With k increasing, the classification accuracy naturally diminishes, confirming the usefulness of the *audio-visual features* for image generation. The interesting result is that the gap in accuracy between the

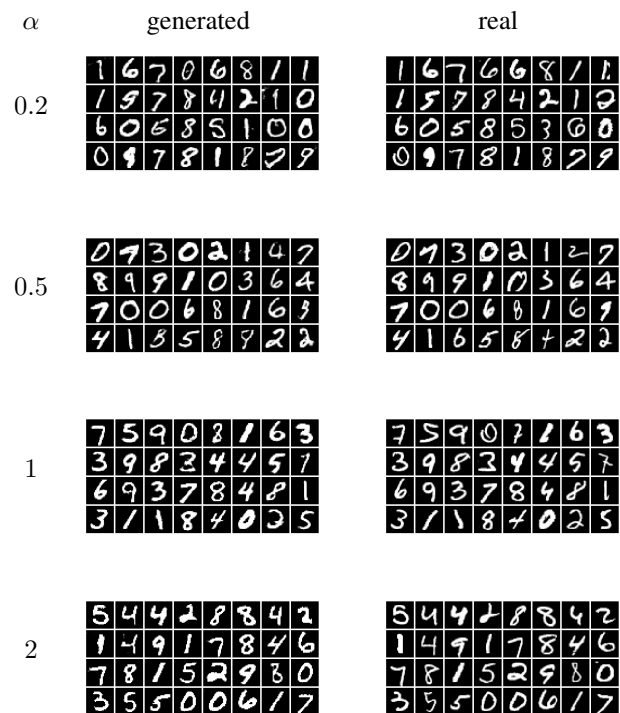


Figure 6. Generated vs. real images at the end of training for different levels of reconstruction loss importance (AIVAEGAN, MNIST-SCD).

models trained on the many-to-one dataset and the one-to-one dataset narrows down and actually disappears for larger numbers of the elements of the latent vector restricted to 0. This suggests that for the many-to-one alignment, the whole set of features is crucial for performance, while the one-to-one alignment results in a model that is more robust to a removal of a small subset of features.

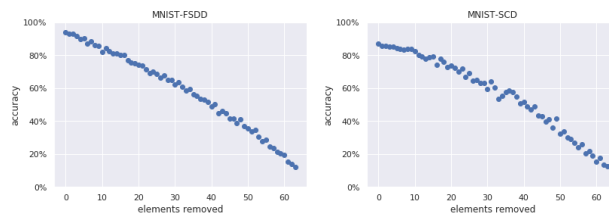


Figure 8. Classification accuracy of a pretrained LeNet5 classifier for AIVAE with different numbers of the elements of the latent vector randomly set to 0.

6. Conclusions

In this work we show that it is possible to generate images based on audio features extracted from sounds. We train cross-modal VAEs and their adversarial extensions on two synthetic datasets and obtain results which suggest that the

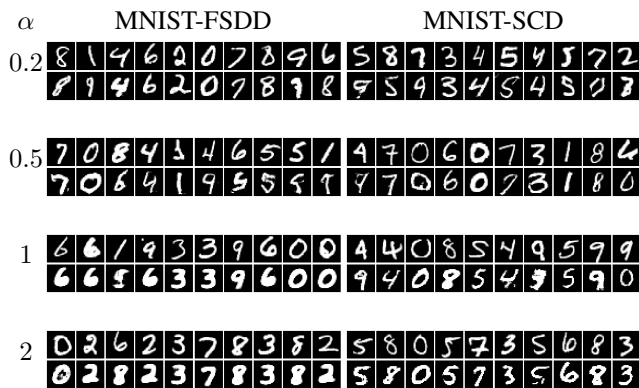


Figure 7. Test-set reconstructions by AIVAEGAN for different levels of reconstruction loss importance. Random, not cherry-picked.

Table 3. LeNet5 architecture.

LENET5
INPUT 32X32
CONV 1X1, 6, STR=5, RELU
MAX POOL 2X2, STR=2
CONV 6X6, 16, STR=5, RELU
MAX POOL 2X2, STR=2
CONV 16X16, 120, STR=5, RELU
FLATTEN 120
FC 84, RELU
FC 10, SOFTMAX
OUTPUT 10

audio-visual features - the subset of relevant visual features corresponding to audio features - are sufficient to generate images similar to the ones from the data space. We also show that the degree of adherence of the generated images to the ones from the data space can be modeled by choosing an appropriate weight for the reconstruction loss. For audio which repeats itself for a given image, our models tend to produce image archetypes. In a setting where each data point is uniquely paired with another one from the other modality, archetypes are weaker and the data retains more diversity without necessarily losing much of the relevant visual features.

Our study provides results in a hitherto underrepresented area of cross-modal learning related to audio-visual data. We show that audio-to-image generation is possible both in a VAE architecture and by adversarially extending it. This provides a new approach toward architectures which could be employed in a cross-modal setting. Additionally, we provide an analysis of the impact the kind of dataset alignment (many-to-one vs. one-to-many) may have on the generated data. It is not hard to imagine scenarios where the generation of archetypes might be of interest (e.g. when we are interested in only the general notion and not a specific

Table 4. Test-set classification accuracy of a pretrained LeNet5 network on images generated by AIVAE.

DATA SET	MNIST-FSDD	MNIST-SCD
ACCURACY	94.2%	86.6%

Table 5. Test-set classification accuracy for a pretrained LeNet5 network on images generated by AIVAEGAN.

DATA SET \ $\alpha =$	0.2	0.5	1	2
MNIST-FSDD	81.0%	80.5%	93.0%	94.3%
MNIST-SCD	66.9%	76.2%	81.7%	81.5%

object) vs. scenarios where diversity could be preferable to strict adherence (e.g. when we are interested in obtaining many examples of one specific notion).

On a more general note, our work provides a method for generating data in an unsupervised manner, which could contribute toward creating a more realistic model of the world in artificial intelligence systems. Generating images from sound could potentially be used in a variety of situations, e.g. to help people with impaired hearing, to visualize sounds, to create art, etc.

Presented results point to several potential lines of research which we plan to consider in our future work. First of all, while in this study we have discounted the possibility of forming one representation per modality rather than one universal shared representation, it might be beneficial to analyze settings where two or more representations are formed with a shared subset as this may allow to retain more relevant features from each analyzed modality. Second of all, the obtained results suggest that the supervisory signal contained in the alignment of datasets may be enough to at least somewhat successfully generate data from one modality based on the aligned data from another modality. This, in turn, suggests the possibility of leveraging a number of unlabeled datasets to obtain shared cross-modal representations. Online streaming services which present their users with videos seem like a natural choice since videos contain naturally aligned audio and visual data. It would be interesting to see extensions handling temporal data such as audio-video streams. Finally, it would be interesting to test the extent to which cross-modal representations can be formed from unaligned datasets, and the extent to which such representations could be used to bind two data points from different modalities.

References

Ackley, D. H., Hinton, G. E., and Sejnowski, T. J. A learning algorithm for boltzmann machines. *Cognitive Science*, 9

- (1):147–169, 1985.
- Arandjelovic, R. and Zisserman, A. Look, listen and learn. October 2017.
- Arandjelovic, R. and Zisserman, A. Objects that sound. September 2018.
- Arjovsky, M., Chintala, S., and Bottou, L. Wasserstein gan. In *International Conference on Machine Learning*, August 2017.
- Bengio, Y., Courville, A., and Vincent, P. Representation learning: A review and new perspectives. *IEEE Transactions on Pattern Analysis and Machine Intelligence*, 35(8):1798–1828, Aug 2013. ISSN 1939-3539.
- Bourlard, H. and Kamp, Y. Auto-association by multilayer perceptrons and singular value decomposition. *Biological Cybernetics*, 59(4):291–294, Sep 1988.
- Brock, A., Donahue, J., and Simonyan, K. Large scale GAN training for high fidelity natural image synthesis. In *International Conference on Learning Representations*, 2019.
- Chen, L., Srivastava, S., Duan, Z., and Xu, C. Deep cross-modal audio-visual generation. In *Proceedings of the on Thematic Workshops of ACM Multimedia 2017, Mountain View, CA, USA, October 23 - 27, 2017*, pp. 349–357, 2017.
- Donahue, J., Krähenbühl, P., and Darrell, T. Adversarial feature learning. In *International Conference on Learning Representations (ICLR)*, 2017.
- Goodfellow, I., Pouget-Abadie, J., Mirza, M., Xu, B., Warde-Farley, D., Ozair, S., Courville, A., and Bengio, Y. Generative adversarial nets. In Ghahramani, Z., Welling, M., Cortes, C., Lawrence, N. D., and Weinberger, K. Q. (eds.), *Advances in Neural Information Processing Systems 27*, pp. 2672–2680. Curran Associates, Inc., 2014.
- Hao, W., Zhang, Z., and Guan, H. Cmcgan: A uniform framework for cross-modal visual-audio mutual generation. In *AAAI Conference on Artificial Intelligence*, 2018.
- Hinton, G. E. and Zemel, R. S. Autoencoders, minimum description length and helmholtz free energy. In *Proceedings of the 6th International Conference on Neural Information Processing Systems, NIPS’93*, pp. 3–10, San Francisco, CA, USA, 1993. Morgan Kaufmann Publishers Inc.
- Hinton, G. E., McClelland, J. L., and Rumelhart, D. E. *Distributed Representations*, pp. 77–109. MIT Press, Cambridge, MA, USA, 1986. ISBN 026268053X.
- Hsu, W.-N. and Glass, J. Disentangling by partitioning: A representation learning framework for multimodal sensory data. arXiv:1805.11264, 2018.
- Kingma, D. P. and Ba, J. Adam: A method for stochastic optimization. ICLR, 2015.
- Kingma, D. P. and Welling, M. Auto-encoding variational bayes. In *Proceedings of the 2nd International Conference on Learning Representations (ICLR)*, 2014.
- Kramer, M. A. Nonlinear principal component analysis using autoassociative neural networks. *AICHE Journal*, 37(2):233–243, 1991.
- Lecun, Y., Bottou, L., Bengio, Y., and Haffner, P. Gradient-based learning applied to document recognition. In *Proceedings of the IEEE*, pp. 2278–2324, 1998.
- Li, C., Gao, S., Deng, C., Xie, D., and Liu, W. Cross-modal learning with adversarial samples. In Wallach, H., Larochelle, H., Beygelzimer, A., d’Alché Buc, F., Fox, E., and Garnett, R. (eds.), *Advances in Neural Information Processing Systems 32*, pp. 10791–10801. Curran Associates, Inc., 2019.
- Lu, J., Batra, D., Parikh, D., and Lee, S. Vilbert: Pre-training task-agnostic visiolinguistic representations for vision-and-language tasks. In Wallach, H., Larochelle, H., Beygelzimer, A., d’Alché Buc, F., Fox, E., and Garnett, R. (eds.), *Advances in Neural Information Processing Systems 32*, pp. 13–23. Curran Associates, Inc., 2019.
- Miyato, T., Kataoka, T., Koyama, M., and Yoshida, Y. Spectral normalization for generative adversarial networks. In *International Conference on Learning Representations*, 2018.
- Müller-Eberstein, M. and van Noord, N. Translating visual art into music. In *International Conference on Computer Vision (ICCV)*, 2019.
- Oord, A. v. d., Dieleman, S., Zen, H., Simonyan, K., Vinyals, O., Graves, A., Kalchbrenner, N., Senior, A., and Kavukcuoglu, K. Wavenet: A generative model for raw audio. arXiv:1609.03499, 2016.
- Radford, A., Metz, L., and Chintala, S. Unsupervised representation learning with deep convolutional generative adversarial networks. In *International Conference on Learning Representations (ICLR)*, May 2016.
- Razavi, A., van den Oord, A., and Vinyals, O. Generating diverse high-fidelity images with vq-vae-2. In Wallach, H., Larochelle, H., Beygelzimer, A., d’Alché Buc, F., Fox, E., and Garnett, R. (eds.), *Advances in Neural Information Processing Systems 32*, pp. 14837–14847. Curran Associates, Inc., 2019.

- Reed, S., Akata, Z., Yan, X., Logeswaran, L., Schiele, B., and Lee, H. Generative adversarial text-to-image synthesis. In *Proceedings of The 33rd International Conference on Machine Learning*, 2016.
- Rumelhart, D. E., Hinton, G. E., and Williams, R. J. *Learning Internal Representations by Error Propagation*, pp. 318–362. MIT Press, Cambridge, MA, USA, 1986. ISBN 026268053X.
- Schmidhuber, J. Learning factorial codes by predictability minimization. *Neural Computation*, 4(6):863–879, Nov 1992. ISSN 0899-7667.
- Shi, Y., N, S., Paige, B., and Torr, P. Variational mixture-of-experts autoencoders for multi-modal deep generative models. In Wallach, H., Larochelle, H., Beygelzimer, A., Alché-Buc, F., Fox, E., and Garnett, R. (eds.), *Advances in Neural Information Processing Systems 32*, pp. 15692–15703. Curran Associates, Inc., 2019.
- Sun, C., Myers, A., Vondrick, C., Murphy, K., and Schmid, C. Videobert: A joint model for video and language representation learning. In *The IEEE International Conference on Computer Vision (ICCV)*, October 2019.
- van den Oord, A., Vinyals, O., and Kavukcuoglu, K. Neural discrete representation learning. In Guyon, I., Luxburg, U. V., Bengio, S., Wallach, H., Fergus, R., Vishwanathan, S., and Garnett, R. (eds.), *Advances in Neural Information Processing Systems 30*, pp. 6306–6315. Curran Associates, Inc., 2017.
- Vincent, P., Larochelle, H., Bengio, Y., and Manzagol, P.-A. Extracting and composing robust features with denoising autoencoders. In *Proceedings of the 25th International Conference on Machine Learning, ICML '08*, pp. 1096–1103, New York, NY, USA, 2008. Association for Computing Machinery. ISBN 9781605582054.
- Wen, Y., Ismail, M. A., Liu, W., Raj, B., and Singh, R. Disjoint mapping network for cross-modal matching of voices and faces. In *International Conference on Learning Representations*, 2019.
- Weston, J., Bengio, S., and Usunier, N. Large scale image annotation: learning to rank with joint word-image embeddings. *Machine Learning*, 81(1):21–35, Oct 2010. ISSN 1573-0565.
- Xing, C., Rostamzadeh, N., Oreshkin, B., and O. Pinheiro, P. O. Adaptive cross-modal few-shot learning. In Wallach, H., Larochelle, H., Beygelzimer, A., d’Alché Buc, F., Fox, E., and Garnett, R. (eds.), *Advances in Neural Information Processing Systems 32*, pp. 4848–4858. Curran Associates, Inc., 2019.